

# Spatial Motifs for Device-to-Device Network Analysis (DNA) in Cellular Networks

Tengchan Zeng\*, Omid Semiari<sup>†</sup>, Walid Saad\*, and My T. Thai<sup>‡</sup>

\*Wireless@VT, Electrical and Computer Engineering Department, Virginia Tech, VA, USA,

<sup>†</sup>Department of Electrical Engineering, Georgia Southern University, Statesboro, GA, USA,

<sup>‡</sup>Department of Computer and Information Science and Engineering, University of Florida, Gainesville, FL, USA,

Emails: \*{tengchan, walids}@vt.edu, <sup>†</sup>osemiari@georgiasouthern.edu, <sup>‡</sup>mythai@cise.ufl.edu.

## Abstract

Device-to-device (D2D) communication is a promising approach to efficiently disseminate critical or viral information. Reaping the benefits of D2D-enabled networks is contingent upon choosing the optimal content dissemination policy subject to resource and user distribution constraints. In this paper, a novel D2D network analysis (DNA) framework is proposed to study the impacts of frequently occurring subgraphs, known as motifs, on D2D network performance and to determine an effective content dissemination strategy. In the proposed framework, the distribution of devices in the D2D network is modeled as a Thomas cluster process (TCP), and two graph structures, the star and chain motifs, are studied in the communication graph. Based on the stochastic properties of the TCP, closed-form analytical expressions for the statistical significance, the outage probability, as well as the average throughput per device, are derived. Simulation results corroborate the analytical derivations and show the influence of different system topologies on the occurrence of motifs and the D2D system throughput. More importantly, the results highlight that, as the statistical significance of motifs increases, the system throughput will initially increase, and, then, decrease. Hence, network operators can obtain statistical significance regions for chain and star motifs that map to the optimal content dissemination performance. Furthermore, using the obtained regions and the analytical expressions for statistical significance, network operators can effectively identify which clusters of devices can be leveraged for D2D communications while determining the number of serving devices in each identified cluster.

## I. INTRODUCTION

The number of mobile devices, such as smartphones and tablets, has significantly increased, and almost half a billion mobile devices were added in 2016 [2]. This growth in mobile devices has been accompanied by a rise in the need for pervasive wireless connectivity in

A preliminary version of this work was presented in part at the IEEE Asilomar Conference on Signals, Systems, and Computers, Pacific Grove, CA, USA, Oct. 2017 [1]. This research was supported by the U.S. National Science Foundation under Grant CNS-1513697.

which users require to access their content of interest anywhere, anytime, and on any device. One effective approach for such large-scale content dissemination is to use device-to-device (D2D) communication links, which enable mobile devices to communicate directly without infrastructure [3]–[5]. By leveraging the physical proximity of device, D2D communications can provide an effective means for disseminating contents (such as disaster alerts, commercial advertisement, and event notifications) to users across a geographical region. However, when deploying D2D communications for content dissemination, one must address two key challenges [3]–[16]: a) designing *content dissemination strategies* for choosing the number of serving devices that can serve as seeds for disseminating content, and b) developing metrics to assess the content dissemination performance under different network topology parameters.

First, in order to choose the optimal set of serving devices, one can leverage a communication graph composed of D2D links and make use of graph-theoretic properties to identify the most influential devices that can store popular content and the number of serving devices is chosen to maximize the overall system throughput [6]–[11]. For example, in [6] and [7], the authors use degree centrality, defined as the number of connected D2D links for every node, and identify the set of nodes with high degree centrality as serving devices. Meanwhile, the works in [8] and [9] focus on the betweenness centrality, which measures the fraction of shortest paths passing through a focal node, to identify the set of serving devices for D2D content dissemination purposes. Moreover, the authors in [10] use the closeness centrality, computed by the sum of distance between a node and all other nodes in the graph, to establish the strategy for choosing the best set of serving devices. Furthermore, in [11], the authors first build the adjacency matrix for D2D communication network, and then choose the set of serving devices by using the eigenvector corresponding to the largest eigenvalue in the adjacency matrix.

Although the works in [6]–[11] exploit the graph-based properties, these works solely focus on the low-order network connectivity, which can only capture the features at the level of individual nodes and edges. In other words, these properties just measure the accumulation of influence from one device on other devices or D2D links. However, for content dissemination, understanding how information propagates among multiple nodes is critical, as such propagation can directly capture the influence of one device on a group of devices. On the other hand, the works in [6]–[11] do not conduct performance analysis for content dissemination under different network topologies.

For analyzing the performance of content dissemination using D2D and deriving tractable

performance metrics for coverage and data rate, it has become customary to use stochastic geometry techniques as done in [12]–[16]. For example, in [12], the authors derive the closed-form expression for the data rate of a cellular network in which D2D receivers are assumed to be located at a fixed distance from their transmitters whose locations are modeled as a Poisson point process (PPP). Also, the authors in [13] derive the outage probability for an arbitrary D2D link in a model where D2D receivers are uniformly distributed in a circular region around the transmitters. Moreover, in [14], to capture the notion of *device clustering*, the authors model the locations of the devices as a Poisson cluster process (PCP), and develop expressions for coverage probability and area spectral efficiency. Furthermore, performance metrics, such as outage probability and average data rate, are also analyzed for systems where the distributions of base stations and devices follow PPP as done in [15] and [16].

Nevertheless, these works in [12]–[16] do not consider multicast and multi-hop communications, which can extend the range of content dissemination and achieve a better performance compared with single-hop D2D links [3]. In addition, these works are restricted to the modeling and analysis of D2D communication, and do not consider any content dissemination policy or the choice of the optimal set of serving devices. Although multicast and multihop communications have been considered, respectively, in [17] and [18], these works do not study more practical scenarios in which both types of communications exist. Moreover, the authors in [17] and [18] are restricted to D2D systems with uniformly and independently distributed BSs and devices. However, due to the similarity of users' content interests, devices can group together within a given area, e.g., a library, and form clusters rather than being independently and uniformly distributed.

The main contribution of this paper is to propose a graph-based D2D network analysis (DNA) framework to determine the content dissemination strategy in clustered D2D networks where both multicast and multi-hop communications exist. In particular, we first develop a framework, based on stochastic geometry, that models the distribution of device groups within the D2D network as a cluster process. Then, we build a D2D communication graph based on the distance distribution among devices and explore frequently occurring network subgraphs, also known as *graph motifs*, to capture content propagation patterns in a group of devices. Next, we theoretically analyze the occurrences for two types of graph motifs, i.e., chain (multi-hop) and star (multicast) motifs, and conduct rigorous performance analysis for D2D and cellular devices. Finally, based on the theoretical analysis, we determine guidelines for designing effective content dissemination

strategies in D2D-enabled cellular networks. To our best knowledge, this is *the first work that exploits network motifs to analyze the performance of content dissemination in D2D-enabled cellular networks*. The novelty of this work lies in the following key contributions:

- We explore occurring network structures, known as graph motifs, to capture content propagation patterns among a group of devices and theoretically analyze the occurrences of different motifs in D2D networks. In particular, we model the distribution of devices as a Thomas cluster process (TCP), where the devices are normally scattered around the central points. Then, based on the distance distribution between two arbitrary devices in the network, we formulate a distance-based graph. Also, we derive tractable expressions for the statistical significance to capture the occurrences of two types of motifs, chain and star motifs that respectively capture multi-hop and multicast communications.
- We conduct a comprehensive performance analysis for both D2D chain and star motifs. In particular, we derive closed-form and tractable expressions for the average throughput for D2D and cellular devices, in presence of motifs. Moreover, we also derive the outage probabilities for both chain and star motifs and provide analytical bounds for the derived expressions.
- Extensive simulation results are used to corroborate the analytical results. In particular, we can observe the influence of different system topologies on the occurrence and the outage probability of motifs and the system throughput. Moreover, the results highlight that as the statistical significance of motifs increases, the system throughput will initially increase, and, then, decrease.
- The proposed framework provides important guidelines for designing effective content dissemination strategies in D2D-enabled cellular networks. In particular, using the derived expressions and the simulation results, network operators can determine the statistical significance regions for different motifs that map to the optimal system throughput. Moreover, by comparing the motifs' statistical significance in each cluster with the optimal regions, the operators can identify which clusters can be optimally leveraged for D2D communications. In addition, based on the analytical derivations on the statistical motif occurrence, one can also determine the number of serving devices in each identified cluster.

The rest of the paper is organized as follows. Section II presents the system model and key assumptions. In Section III and Section IV, we conduct graph motifs based analysis for D2D

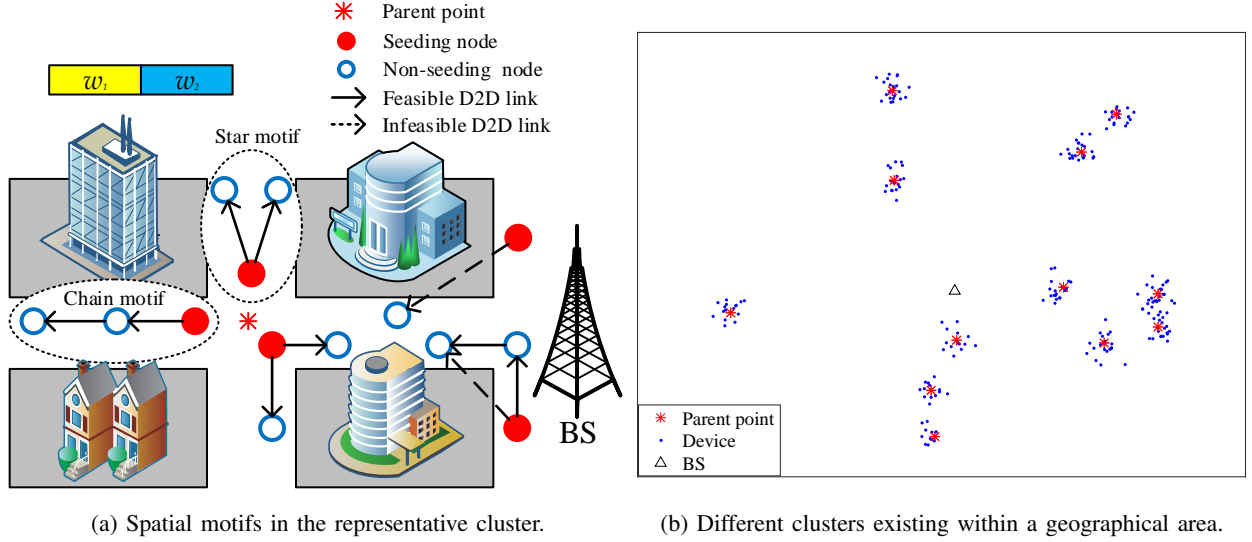


Fig. 1. System model that follows a TCP.

networks and develop the performance-related metrics. Simulation results are provided in Section V and conclusions are drawn in Section VI.

## II. SYSTEM MODEL

Consider a cellular network composed of a single BS and a number of devices that can communicate with the BS over cellular links as well as directly exchange information with one another via D2D communications, as shown in Fig. 1(a). Here, devices with injected contents from the BS are referred to as *seeding nodes*, and those that obtain the content from nearby devices are called *non-seeding nodes*. Moreover, due to the similarity of users' interests, devices can concentrate at the same area, such as a library or a stadium [7]–[11], and the grouped devices will form clusters. As done in [19], to avoid the interference between cellular and D2D links, we consider a D2D overlay system in which the available bandwidth  $w$  is partitioned into  $w_1 = \beta w$  for D2D links and  $w_2 = (1 - \beta)w$  for cellular links, where  $\beta \in (0, 1)$ .

To capture the non-uniform, cluster-based distribution of devices in the network, we consider a TCP composed of a parent point process and a daughter point process [20]. In particular, as shown in Fig. 1(b), we model the distribution of the parent points (center points of the clusters) as a PPP  $\Phi_p$  with density  $\lambda_p$ . Also, the daughter points (devices) in each cluster are normally scattered with variance  $\sigma^2$  around the corresponding parent point  $x \in \Phi_p$  [20]. Note that the locations of daughter points, with respect to the corresponding parent point, are independent and identically distributed (i.i.d.) variables [20].

### A. D2D Communication Graph

As shown in Fig. 1(a), we arbitrarily select a cluster with parent point  $x_r \in \Phi_p$ , considered as a *representative cluster*  $C_r$ . In cluster  $C_r$ , seeding nodes can disseminate popular contents to other devices via D2D links. Nonetheless, due to limited transmit power, devices that belong to cluster  $C_r$  will not communicate with other clusters. Hence, in cluster  $C_r$ , we can model the D2D network as a directed acyclic graph  $G = (\Phi_{x_r}, \mathcal{E}_{x_r})$ , whose vertices are devices in the set  $\Phi_{x_r}$  and whose edges, within the set  $\mathcal{E}_{x_r}$ , are D2D links among devices in the cluster. In particular, each D2D link can be defined as a 2-tuple edge,  $e = \langle i, j \rangle$ , where device  $i$  and device  $j$  are the transmitter and the receiver, respectively,  $i, j \in \Phi_{x_r}$ . Also, as done in [21] and [22], we assume that no edge exists between a pair of vertices in graph  $G$  if their distance exceeds the maximum value  $s_{th}$ . Moreover, if there exists a graph  $G' = (\Phi'_{x_r}, \mathcal{E}'_{x_r})$  with  $\Phi'_{x_r} \subseteq \Phi_{x_r}$  and  $\mathcal{E}'_{x_r} \subseteq \mathcal{E}_{x_r}$ , the graph  $G'$  is a subgraph of  $G$ . For analytical tractability, we assume that the number of devices in each cluster is  $N$ . As will be clear from the following discussion, although the total number of devices in each cluster is the same, the number of D2D links varies from one cluster to another, which maintains generality of the model.

By focusing on cluster  $C_r$ , we can observe that groups of D2D links can form various subgraphs with different structures, which can show how the content propagates among a group of devices. For example, as shown in Fig. 1(a), two D2D links can share the same transmitter, and the receiver of one link can act as the transmitter of another D2D link. To characterize D2D subgraphs appearing in the network, we exploit the notion of *graph motifs*, defined as frequently occurring subgraphs. The frequency of occurrence of motifs is typically measured with respect to a baseline system such as a random graph built by randomly assigning D2D links to pairs of arbitrary devices [23]. In addition, to capture the occurrence of different motifs, one can measure the statistical significance for each motif using the notion of a *Z-score* [24]:

$$Z = \frac{c_o - c_r}{\varepsilon_r}, \quad (1)$$

where  $c_o$  is the number of occurrences of a given motif in the network, and  $c_r$  and  $\varepsilon_r$  denote, respectively, the mean and the standard deviation of motif's occurrence in the baseline system. For the baseline system, we use a random graph model that shares the same total number of D2D links existing in graph  $G$ , but randomly rewires each link between an arbitrary pair of devices [25]. For example, if there are  $c_o$  motifs where one seeding node sends data to two non-seeding nodes, the total number of edges in the baseline system will be  $2c_o$ . As a result, the edge between

any pair of devices in the baseline system occurs with the same probability  $2c_0/\binom{N}{2}$ . Using the properties of the binomial distribution, we can derive  $c_r = \lfloor N/3 \rfloor \binom{3}{1} (2c_0/\binom{N}{2})^2 (1 - 2c_0/\binom{N}{2})$  and  $\varepsilon_r = \lfloor N/3 \rfloor \binom{3}{1} (2c_0/\binom{N}{2})^2 (1 - 2c_0/\binom{N}{2}) \left(1 - \binom{3}{1} (2c_0/\binom{N}{2})^2 (1 - 2c_0/\binom{N}{2})\right)$ , where  $\lfloor x \rfloor$  is the floor function of  $x$  and  $\binom{x}{y}$  denotes the number of  $y$ -combinations in a set with  $x$  elements. Furthermore, we can observe that  $\frac{dZ}{dc_0} > 0$ , when  $c_0 \geq 1$ , indicating that the  $Z$ -score is an increasing function of the motif occurrence parameter  $c_0$ .

In addition, we assume that each seeding device can disseminate content to multiple non-seeding devices, and non-seeding devices are capable of forwarding the content to others. Therefore, as illustrated in Fig. 1(a), for any group of three devices, we can observe two types of communication motifs – the *star motif* and the *chain motif*. The star motif can be viewed as a *multicast* link in which the seeding device disseminates its content to two non-seeding devices, and is captured by two edges sharing the same first element in the communication graph. Meanwhile, the chain motif can be considered as a two-hop D2D link. In particular, the seeding device will first send its content to a non-seeding device in one time slot, which functions as a relay propagating the content to another non-seeding device in the next time slot. Similarly, for the chain motif in the graph, there exists two edges connecting three devices, and the second element of one edge is the first element of the next edge. Here, we focus on three-device motifs, since larger motifs can always be constructed using smaller motifs, and, hence, our framework can easily extend to any other graph structures.

### B. Channel Model and Interference Analysis

For the D2D link  $(i, j)$ , from device  $i \in \Phi_{x_r}$  to  $j \in \Phi_{x_r}$ , in cluster  $C_r$  centred at  $x_r \in \Phi_p$ , the received power is given by  $P_{ij} = P_t h_{ij} d_{ij}^{-\alpha}$ , where  $P_t$  is the transmit power of each device,  $h_{ij}$  is the channel gain that follows a Rayleigh fading distribution,  $d_{ij}$  is the corresponding distance between any two devices  $i$  and  $j$ , and  $\alpha$  is the path loss exponent. Similar to the bandwidth allocation in [26], in a star motif, we assume that the two D2D links will split the frequency resources evenly and each link uses half of the bandwidth,  $\frac{w_1}{2}$ . Meanwhile, in a chain motif, the first and second D2D links will reuse the same resource,  $w_1$ , at two consecutive time slots. Therefore, due to the co-channel deployment of D2D links, the receiving nodes will encounter interference from other D2D links, irrespective of their motif types. We designate the interference on device  $j$  generated from devices in cluster  $C_r$  as the *intra-cluster interference*  $I_{j-\text{intra}}^{x_r}$ , and

the interference from devices within other clusters as *the inter-cluster interference*  $I_{j-\text{inter}}^{x_r}$ . The two types of interference are given by:

$$I_{j-\text{intra}}^{x_r} = \sum_{y \in \Phi_{x_r} \setminus \{i,j\}} \mathbb{1}_y P_t h_{yj} d_{yj}^{-\alpha}, \quad I_{j-\text{inter}}^{x_r} = \sum_{x \in \Phi_p \setminus x_r} \sum_{y \in \Phi_x} \mathbb{1}_y P_t h_{yj} d_{yj}^{-\alpha}, \quad (2)$$

where the indicator variable  $\mathbb{1}_y = 1$  if device  $y$  is transmitting data to other device via D2D link; otherwise,  $\mathbb{1}_y = 0$ . For a large D2D network, the thermal noise power at the receiver will be substantially smaller than the received interference power [27]. Thus, the expression of the signal-to-interference-plus-noise ratio (SINR) of the D2D link can be approximated as

$$\delta_{ij} \approx \frac{P_t h_{ij} d_{ij}^{-\alpha}}{I_{j-\text{intra}}^{x_r} + I_{j-\text{inter}}^{x_r}}. \quad (3)$$

Since we consider a single-cell scenario and the BS will transmit contents to seeding devices in different time slots, the seeding devices will experience no interference and their signal-to-noise ratio (SNR) will be:

$$\delta_{bj} = \frac{P_b h_{bj} d_{bj}^{-\alpha}}{P_n}, \quad (4)$$

where  $P_b$  is the transmission power of the BS,  $h_{bj}$  is the channel gain that follows a Rayleigh distribution,  $d_{bj}$  represents the distance between the BS and device  $j$ , and  $P_n$  captures the power of the background noise. Moreover, we can find the achievable data rate  $R$  for D2D links and cellular links, according to  $R = w_3 \log_2(1 + \delta)$ , where  $w_3$  is the assigned bandwidth.

### C. Relationship between the Occurrence of Motifs and the D2D System Throughput

For each cluster, the BS can collect the occurrence of different communication motifs and calculate the data rate of each device. Due to the co-channel deployment of D2D links, interference will increase as the frequency of occurrence of any given motif increases. As a result, as shown in Section II-A, the  $Z$ -score is an increasing function of the occurrence  $z_o$  of motifs, and, hence, the interference will increase as the  $Z$ -score increases. Thus, for clusters having higher  $Z$ -scores, content dissemination via D2D communications will experience a high interference, thereby degrading the dissemination throughput. On the other hand, for clusters with a smaller  $Z$ -score, only a limited number of D2D links can be formed, resulting in a low spectral reuse. Therefore, we need to find the  $Z$ -score region, which can yield an optimal system performance. This  $Z$ -score region can allow identifying clusters that can be used for D2D communications by comparing any given  $Z$ -score of the clusters with the optimal region. Moreover, the number

of seeding devices in each identified cluster can be determined based on the number of cellular devices.

However, due to the lack of closed-form expressions that link the  $Z$ -score and the wireless throughput, directly finding the  $Z$ -score region that yields the optimal system performance is challenging. Nevertheless, we can observe that the value of the  $Z$ -score depends on number of devices  $N$ , their locations, and the maximum communication distance  $s_{th}$ . In addition, the system throughput is also a function of these three parameters. Therefore, instead of finding a direct relationship between the  $Z$ -score and the system throughput, one can alternatively determine the analytical expressions of the  $Z$ -score and the system throughput as function of their common parameters. Using such analytical expressions, the BS can collect data on the  $Z$ -score and the system throughput corresponding to the same parameter settings, and further observe how the system throughput changes as the  $Z$ -score of motifs varies. The changes of the system throughput as function of the  $Z$ -score can enable network operators to disclose the relationship between the occurrence of motifs and the system performance, and further determine the  $Z$ -score region which maps to the optimal system throughput. Next, we will first leverage the distance distribution among devices and the stochastic properties inherent in the TCP to derive tractable expressions for the  $Z$ -scores of chain and star motifs and the system throughput. Also, we will further identify the hidden relationship between motifs and the system performance based on simulation results and determine the content dissemination strategy for clustered networks.

### III. STATISTICAL SIGNIFICANCES OF STAR AND CHAIN MOTIFS

In this section, for an arbitrarily chosen group of three devices in cluster  $C_r$ , we leverage the distance distribution between any two randomly and uniformly selected points to derive the probability of the content dissemination pattern among three devices being either a star or chain motif. Based upon the probability of occurrence, we can derive closed-form expressions for the  $Z$ -scores.

#### A. Distance Distribution

We arbitrarily select a group of three devices in cluster  $C_r$ , and due to the stationarity of the TCP, we treat an arbitrary device out of these three devices as *a typical point* located at the origin. In addition, we assume that the location of the parent point is at  $x_r \in \Phi_p$ , and the other two devices are located at  $y_1$  and  $y_2$  relative to the parent point. Therefore, according to the

definition of the TCP in Section II,  $y_1$  and  $y_2$  are distributed according to a symmetric normal distribution with the variance  $\sigma^2$  around the parent point  $x_r$ , and the parent point also follows a zero mean symmetric normal distribution with the variance  $\sigma^2$  relative to the origin point. Additionally,  $x_r$ ,  $y_1$ , and  $y_2$  are i.i.d. variables,  $x_r, y_1, y_2 \in \mathbb{R}^2$ .

Furthermore, we denote  $\{\mathcal{D}_i\}_{i=1, \dots, N-1}$  as the distance set from the typical point to another uniformly selected point in the same cluster. In particular, the realization of  $\{\mathcal{D}_i\}_{i=1, \dots, N-1}$  is  $d_i = \|x_r + y_i\|, i = 1, \dots, N-1$ . Conditioned on the distance from the typical point to the parent point  $s_r = \|x_r\|$ , the probability density function (PDF) of  $d_i$  follows a Rician distribution [27]:

$$f_D(d_i, s_r; \sigma^2) = \frac{d_i}{\sigma^2} \exp\left(-\frac{d_i^2 + s_r^2}{2\sigma^2}\right) I_0\left(\frac{d_i s_r}{\sigma^2}\right), d_i, s_r \geq 0, \quad (5)$$

where  $I_0(\cdot)$  is the modified Bessel function of first kind with zero order. Conditioned on  $s_r = \|x_r\|$ , the elements in  $\mathcal{D}_i$  are also i.i.d. variables as shown in [27]. Moreover, the authors in [27] also conclude that when the distances from the typical point to the parent points of other clusters are a fixed value, the distances between the typical device at the origin and the devices in other clusters are also i.i.d. variables and follow Rician distributions. As it will be clear from the following discussion, we use this property to calculate inter-cluster interference. In addition, according to the definition of the TCP, the distance  $s_r$  follows a Rayleigh distribution with scale parameter  $\sigma$  and with the following PDF:

$$f_S(s_r; \sigma^2) = \frac{s_r}{\sigma^2} \exp\left(-\frac{s_r^2}{2\sigma^2}\right), s_r \geq 0. \quad (6)$$

### B. Probability of Occurrence of Motifs

Based on the distance distribution obtained in Section III-A, we can derive the probability with which a group of three arbitrary devices will form either a chain or star motif. First, we can observe that, for both chain and star motifs, there is a node capable of directly communicating with the other two devices. Hence, if we consider a device with two direct D2D links as a typical point located at the origin, we can express the distance from the typical point to the other two uniformly and randomly selected devices as the norm of  $m = x_r + y_1 \in \mathbb{R}^2$ , and  $n = x_r + y_2 \in \mathbb{R}^2$ , where  $m = (m^{(1)}, m^{(2)})$ ,  $n = (n^{(1)}, n^{(2)})$ , and  $x_r = (x_r^{(1)}, x_r^{(2)})$ . In a TCP,  $y_1$  and  $y_2$  are zero mean complex Gaussian random variables relative to  $x_r$ . Hence,  $m^{(1)} \sim \mathcal{N}(x_r^{(1)}, \sigma^2)$ ,  $n^{(1)} \sim \mathcal{N}(x_r^{(1)}, \sigma^2)$ ,  $m^{(2)} \sim \mathcal{N}(x_r^{(2)}, \sigma^2)$ , and  $n^{(2)} \sim \mathcal{N}(x_r^{(2)}, \sigma^2)$ . In addition,  $x_r^{(1)} \sim \mathcal{N}(0, \sigma^2)$ , and  $x_r^{(2)} \sim \mathcal{N}(0, \sigma^2)$ . Thus,  $s_1 = \|m\|$  and  $s_2 = \|n\|$  follow the Rayleigh distribution. Due to the common element,  $x_r$ , in  $m$  and  $n$ , the distances  $s_1$  and  $s_2$  are also correlated. Based on the

distribution and correlation between  $s_1$  and  $s_2$ , next, we can obtain the joint probability of both  $s_1$  and  $s_2$  being smaller than  $s_{th}$ .

**Theorem 1.** *Given that  $s_1 = ||m||$  and  $s_2 = ||n||$  follow Rayleigh distributions and are correlated, the joint probability of both  $s_1 = ||m||$  and  $s_2 = ||n||$  being smaller than  $s_{th}$  is:*

$$\mathbb{P}_{S,S}(s_{th}, s_{th}) = \frac{3}{4} \sum_{k=0}^{\infty} \left( \left( \frac{1}{2} \right)^k \frac{\gamma \left( 1 + k, \frac{s_{th}^2}{3\sigma^2} \right)}{(k!)} \right)^2, \quad (7)$$

where  $\gamma(\cdot, \cdot)$  refers to the lower incomplete gamma function, defined as  $\gamma(a, b) = \int_0^b c^{a-1} e^{-c} dc$ .

*Proof:* To calculate the probability of both  $s_1 = ||m||$  and  $s_2 = ||n||$  being smaller than the distance threshold  $s_{th}$ , we first calculate the correlation existing between  $m$  and  $n$  as

$$\rho = \frac{\text{cov}(m, n)}{\epsilon_m \epsilon_n} = \frac{\text{cov}(m, n)}{\sqrt{\text{cov}(m, m)} \sqrt{\text{cov}(n, n)}} = \frac{1}{2}. \quad (8)$$

where  $\epsilon_m$  and  $\epsilon_n$  are the standard deviations for  $m$  and  $n$ , respectively. Then, due to the fact that both  $||m||$  and  $||n||$  follow Rayleigh distribution, we are able to have the joint cumulative density function (CDF) as [28]

$$\mathbb{P}_{S,S}(s_1, s_2) = \frac{3}{4} \sum_{k=0}^{\infty} \left( \frac{1}{4} \right)^k \frac{\gamma \left( 1 + k, \frac{s_1^2}{3\sigma^2} \right) \gamma \left( 1 + k, \frac{s_2^2}{3\sigma^2} \right)}{k! \Gamma(k+1)}, s_1 \geq 0, s_2 \geq 0, \quad (9)$$

where  $\Gamma(\cdot)$  represents to the complete gamma function, defined as  $\Gamma(a) = (a-1)!$ . After replacing  $s_1$  and  $s_2$  with  $s_{th}$  and simplifications, we can obtain the joint CDF shown in (7). ■

In (7),  $\mathbb{P}_{S,S}(s_{th}, s_{th})$  represents the probability that a typical device can build D2D links with two other devices uniformly and randomly chosen from the cluster, irrespective of the link direction. Since a receiving device cannot access the content from multiple transmitters at the same time, and a transmitter can spread content to at most two devices simultaneously,  $\mathbb{P}_{S,S}(s_{th}, s_{th})$  is the probability with which any three devices can form either the star motif or the chain motif. For ease of exposition, we use the term “three-node motifs” to refer to the union of the star and chain motifs, and replace  $\mathbb{P}_{S,S}(s_{th}, s_{th})$  with  $\mathbb{P}_{S,S}$  hereinafter. Moreover, we assume that the probability of one three-node motif being a star motif is  $\theta$ ,  $0 < \theta < 1$ , and the probability of forming a chain motif will be  $1 - \theta$ .

### C. Z-scores for chain and star motifs

To calculate the Z-scores for the chain and star motifs, we must derive the occurrence of these two motifs in cluster  $C_r$  and compare it with the baseline system. In particular, the maximum number of groups of three devices is  $N_m = \lfloor \frac{N}{3} \rfloor$ , where any arbitrary two groups do not share common devices and devices in each group are randomly and uniformly selected. Therefore, we can express the probability of  $n$  groups of three-node motifs existing in a cluster as  $\binom{N_m}{n} (\mathbb{P}_{S,S})^n (1 - \mathbb{P}_{S,S})^{N_m - n}$ ,  $n \leq N_m$ . Using the properties of the binomial distribution, the expected number  $c_o$  of three-node motifs in the network with distance will be  $c_o = N_m \times \mathbb{P}_{S,S}$ . Accordingly, the expected numbers of occurrence for the star and chain motifs are give by

$$c_o^{\text{star}} = \theta N_m \times \mathbb{P}_{S,S}, \quad c_o^{\text{chain}} = (1 - \theta) N_m \times \mathbb{P}_{S,S}. \quad (10)$$

For the baseline system, the total number of D2D links is equal to the one in the considered system. In particular, since the number of D2D links in each three-node motif is two, the expected number of D2D links in the baseline system is  $2c_o$ . Therefore, we can derive the probability of one pair of arbitrary devices being connected by a D2D link in the baseline system as follows:

$$\mathbb{P}_r = \frac{2c_o}{\binom{N_m}{2}} = \frac{4\mathbb{P}_{S,S}}{N_m - 1}. \quad (11)$$

In this case, the probability with which three devices form a three-node motif is  $\binom{3}{1} (\mathbb{P}_r)^2 (1 - \mathbb{P}_r)$ . Furthermore, the probabilities of being a star motif or a chain motif in the baseline system are  $3\theta(\mathbb{P}_r)^2(1 - \mathbb{P}_r)$ , and  $3(1 - \theta)(\mathbb{P}_r)^2(1 - \mathbb{P}_r)$ , respectively. Similarly, by using the binomial distribution, we can express the mean  $c_r^{\text{star}}$  and the standard deviation  $\varepsilon_r^{\text{star}}$  for the star motif and the counterparts  $c_r^{\text{chain}}$  and  $\varepsilon_r^{\text{chain}}$  for the chain motif in the baseline system as

$$c_r^{\text{star}} = \frac{48\theta N_m (\mathbb{P}_{S,S})^2 (N_m - 1 - 4\mathbb{P}_{S,S})}{(N_m - 1)^3}, \quad (12)$$

$$c_r^{\text{chain}} = \frac{48(1 - \theta) N_m (\mathbb{P}_{S,S})^2 (N_m - 1 - 4\mathbb{P}_{S,S})}{(N_m - 1)^3}, \quad (13)$$

$$\varepsilon_r^{\text{star}} = \sqrt{\frac{48\theta N_m (\mathbb{P}_{S,S})^2 (N_m - 1 - 4\mathbb{P}_{S,S})}{(N_m - 1)^3} \left( 1 - \frac{48\theta N_m (\mathbb{P}_{S,S})^2 (N_m - 1 - 4\mathbb{P}_{S,S})}{(N_m - 1)^3} \right)}, \quad (14)$$

$$\varepsilon_r^{\text{chain}} = \sqrt{\frac{48(1 - \theta) N_m (\mathbb{P}_{S,S})^2 (N_m - 1 - 4\mathbb{P}_{S,S})}{(N_m - 1)^3} \left( 1 - \frac{48(1 - \theta) (\mathbb{P}_{S,S})^2 (N_m - 1 - 4\mathbb{P}_{S,S})}{(N_m - 1)^3} \right)}. \quad (15)$$

After obtaining the occurrence information for both motifs in cluster  $C_r$  and the baseline system, we can derive the Z-scores for both motifs.

**Remark 1.** By using (1), (10) and (12)-(15), the closed-form expressions of  $Z$ -scores for both motifs in the D2D system can be determined. In fact, (10) captures the expected number of occurrences for chain and star motifs can be derived in cluster  $C_r$ . Also, (12)-(15) represent the mean and standard variance of the occurrences for both motifs in the baseline system.

As observed from Theorem 1, the joint probability  $\mathbb{P}_{S,S}$  is a function of the total number of devices  $N$ , the distribution variance  $\sigma^2$ , and the maximum allowable distance  $s_{th}$ . Therefore, we can conclude that the value of the  $Z$ -score is also dependent on  $N$ ,  $\sigma^2$ , and  $s_{th}$ .

#### IV. EXPECTED AVERAGE THROUGHPUT AND OUTAGE PROBABILITY

To analyze the performance of the content dissemination strategy under different clustered network topology parameters, we use the distance distribution properties inherent in the TCP to calculate the expected throughput for D2D and cellular devices. Moreover, the outage probabilities for the chain and star motifs are also derived.

##### A. Expected Throughput for Non-Seeding Devices in the Star Motif

As shown in Fig. 2, we choose an arbitrary star motif as a representative star motif  $M_s$ . In motif  $M_s$ , the two receiving devices,  $j$  and  $k$ , will access data via D2D links from the seeding device,  $i$ , located at the origin. Moreover, we assume that the set of seeding devices in star motifs as  $\mathcal{T}_x$  in the cluster  $x \in \Phi_p$ , and the number of elements in  $\mathcal{T}_x$  cannot be greater than  $N_m$ .

Next, we take device  $j$  as an example and conduct Laplace transforms for the intra- and inter-cluster interference encountered by device  $j$ . Based on the derived Laplace transforms, we can study the performance-related metrics, such as the outage probability and the expected throughput. According to the stationarity of the TCP and the symmetry between the two receiving devices in the star motif, the Laplace transforms of the intra- and the inter-cluster interference for device  $j$  can apply to another device  $k$  and receiving devices in other star motifs.

**Lemma 1.** For device  $j$  in the star motif, the Laplace transform of the intra-cluster interference can be expressed as

$$\mathcal{L}_{j\text{-intra}}^{\text{star}}(s) = \left( \int_0^\infty \frac{1}{1 + sP_tv_1^{-\alpha}} f_{V_1}(v_1) dv_1 \mathbb{P}_{S,S} + 1 - \mathbb{P}_{S,S} \right)^{N_m-1}, \quad (16)$$

where  $f_{V_1}(v_1) = f_S(v_1; 2\sigma^2)$ ,  $v_1 \geq 0$ .



Considering that content dissemination within a star motif will not occur an outage if and only if the SINR for both D2D links in the star motif exceed the minimum requirement  $\delta_{\text{th}}$ , then the outage probability for the star motif can be derived as follows.

**Theorem 2.** *The outage probability for the star motif is given by:*

$$\mathbb{P}_{\text{outage}}^{\text{star}}(\delta_{\text{th}}) = 1 - \left( \int_0^\infty \mathcal{L}_{j\text{-inter}}^{\text{star}} \left( \frac{\delta_{\text{th}}}{P_t} r_1^\alpha \right) \mathcal{L}_{j\text{-intra}}^{\text{star}} \left( \frac{\delta_{\text{th}}}{P_t} r_1^\alpha \right) f_{R_1}(r_1) dr_1 \right)^2, \quad (20)$$

where  $f_{R_1}(r_1) = f_S(r_1; 2\sigma^2)$ ,  $r_1 \geq 0$ ,

*Proof:* We first calculate the SINR distribution for a D2D link to obtain the probability of a D2D link meeting the minimum SINR requirement:

$$\begin{aligned} \mathbb{P}_j^{\text{star}}(\delta_{\text{th}}) &= \mathbb{E}(\mathbb{P}\{\delta_j > \delta_{\text{th}}\}) \\ &= \mathbb{E} \left[ \mathbb{P} \left( h_{ij} > \frac{\delta_{\text{th}}}{P_t} (I_{j\text{-intra}}^{x_r} + I_{j\text{-inter}}^{x_r}) ||x_r + y_j||^\alpha \right) \right] \\ &\stackrel{(a)}{=} \mathbb{E} \left[ \mathbb{E} \left[ -\exp \left( \frac{\delta_{\text{th}}}{P_t} (I_{j\text{-intra}}^{x_r} + I_{j\text{-inter}}^{x_r}) ||x_r + y_j||^\alpha \right) \right] \right] \\ &\stackrel{(b)}{=} \int_0^\infty \mathcal{L}_{j\text{-inter}}^{\text{star}} \left( \frac{\delta_{\text{th}}}{P_t} r_1^\alpha \right) \mathcal{L}_{j\text{-intra}}^{\text{star}} \left( \frac{\delta_{\text{th}}}{P_t} r_1^\alpha \right) f_{R_1}(r_1) dr_1, \end{aligned} \quad (21)$$

where (a) follows the fact that the channel gain  $h_{ij} \sim \exp(1)$  for a Rayleigh fading channel. In (b), we substitute  $r_1$  with  $||x_r + y_j||$  and use polar coordinates. Note that the probability in (21) can also apply to the link between device  $i$  to  $k$ , due to the symmetry between device  $j$  and  $k$ . Since outage will not occur when the SINR of both links exceed the threshold  $\delta_{\text{th}}$ , we can use the probability in (21) for both D2D links in the star motif to derive the outage probability in (20). ■

Since  $R_j = \frac{w_1}{2} \log_2(1 + \delta_j)$ ,  $R_j < R$  will yield  $\delta_j < 2^{\frac{2R}{w_1}} - 1$ . Thus, after replacing  $\delta_{\text{th}}$  with  $2^{\frac{2R}{w_1}} - 1$  in (21), we can have the CDF of the throughput for receiving devices in the star motif.

**Corollary 3.** *Based on the distribution of the SINR, the CDF of the throughput for receivers in the star motif can be derived as follows:*

$$\mathbb{P}(R_j < R) = 1 - \int_0^\infty \mathcal{L}_{j\text{-inter}}^{\text{star}} \left( \frac{2^{\frac{2R}{w_1}} - 1}{P_t} r_1^\alpha \right) \mathcal{L}_{j\text{-intra}}^{\text{star}} \left( \frac{2^{\frac{2R}{w_1}} - 1}{P_t} r_1^\alpha \right) f_{R_1}(r_1) dr_1. \quad (22)$$

By using the relationship between the CDF and the expected value, we are able to obtain the expected throughput of receiving devices in the star motif in the following corollary.

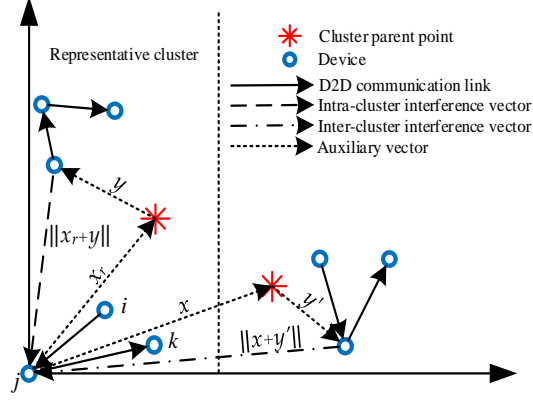


Fig. 3. Illustration of the inter- and intra-cluster interference to the representative chain motif.

**Corollary 4.** *The expected throughput for receivers in the star motif is given by:*

$$\begin{aligned}
 E_{\text{star}} &= \int_0^\infty (1 - P(R_j < R)) dR \\
 &= \int_0^\infty \int_0^\infty \mathcal{L}_{j\text{-inter}}^{\text{star}} \left( \frac{2^{\frac{2R}{w_1}} - 1}{P_t} r_1^\alpha \right) \mathcal{L}_{j\text{-intra}}^{\text{star}} \left( \frac{2^{\frac{2R}{w_1}} - 1}{P_t} r_1^\alpha \right) f_{R_1}(r_1) dr_1 dR. \quad (23)
 \end{aligned}$$

#### B. Expected Throughput for Non-Seeding Devices in the Chain Motif

As illustrated in Fig. 3, we also choose an arbitrary *representative chain motif*  $M_c$  in cluster  $C_r$ . In motif  $M_c$ , the seeding device  $i$  first transmits its data to  $j$ , which is at the origin and will subsequently propagate the data to device  $k$ . Similar to the receiving devices in the star motif, device  $k$  in a chain motif also accesses its content from the transmitter at the origin. Therefore, the Laplace transforms of the intra- and inter-cluster interference given by (16) and (18), and the probability in (21) can be directly applied to the D2D link between device  $j$  and  $k$ . In contrast, due to the different assigned bandwidth, the CDF and the expected throughput must be re-calculated. Nevertheless, unlike device  $k$ , device  $j$  located at the origin has different distance distribution to the serving device and the devices that generate interference from receiving nodes in the star motifs. Hence, to obtain the expression of the throughput, we need to derive the Laplace transforms of the intra- and inter-cluster interference for receiving device  $j$  in the chain motif.

**Lemma 3.** *For the typical device  $j$  in the chain motif, the Laplace transform of the intra-cluster interference, conditioned on the distance from the typical point to the parent point  $s_r = ||x_r||$ , is given by*

$$\mathcal{L}_{j\text{-intra}}^{\text{chain}}(s|s_r) = \left( \int_0^\infty \frac{1}{1 + sP_t v_3^{-\alpha}} f_{V_3}(v_3|s_r) dv_3 \mathbb{P}_{S,S} + 1 - \mathbb{P}_{S,S} \right)^{N_m-1}, \quad (24)$$

where  $f_R(v_3|s_r) = f_D(v_3, s_r; \sigma^2)$ ,  $v_3 \geq 0$ .

*Proof:* See Appendix E. ■

**Corollary 5.** *After using the proof in Appendix B, the lower bound of the intra-cluster interference can be expressed as:*

$$\mathcal{L}_{j\text{-intra}}^{\text{chain}}(s|s_r) \geq 1 - (N_m - 1) \int_0^\infty \frac{sP_t}{v_3^\alpha + sP_t} f_D(v_3, s_r; \sigma^2) dv_3 \mathbb{P}_{S,S}. \quad (25)$$

**Lemma 4.** *For the device  $j$  in the chain motif, the Laplace transform of the inter-cluster interference is given by*

$$\mathcal{L}_{j\text{-inter}}^{\text{chain}}(s) = \exp \left( -\lambda_p 2\pi \int_0^\infty \left( 1 - \left( \int_0^\infty \frac{1}{1 + sP_t v_4^{-\alpha}} f_{V_4}(v_4|t) dv_4 \mathbb{P}_{S,S} + 1 - \mathbb{P}_{S,S} \right)^{N_m} \right) t dt \right), \quad (26)$$

where  $f_{V_4}(v_4|t) = f_D(v_4, t; \sigma^2)$ ,  $v_4 \geq 0$ .

*Proof:* See Appendix F. ■

**Corollary 6.** *After using the proof in Appendix D, the lower bound of the inter-cluster interference experienced by the link from  $i$  to  $j$  is given by*

$$\mathcal{L}_{j\text{-inter}}^{\text{chain}}(s) \geq \exp \left( -\lambda_p 2\pi N_m \frac{(sP_t)^{\frac{2}{\alpha}} \pi \csc \left( \frac{2\pi}{\alpha} \right)}{\alpha} \mathbb{P}_{S,S} \right). \quad (27)$$

Therefore, for a device  $j$ , we can obtain the SINR distribution, which allows deriving the outage probability of a chain motif in the following theorem.

**Theorem 3.** *The outage probability of the chain motif can be calculated as*

$$\begin{aligned} \mathbb{P}_{\text{outage}}^{\text{chain}}(\delta_{\text{th}}) &= 1 - P_k^{\text{star}}(\delta_{\text{th}}) P_j^{\text{chain}}(\delta_{\text{th}}) \\ &= 1 - \left( \int_0^\infty \mathcal{L}_{j\text{-inter}}^{\text{star}} \left( \frac{\delta_{\text{th}}}{P_t} r_1^\alpha \right) \mathcal{L}_{j\text{-intra}}^{\text{star}} \left( \frac{\delta_{\text{th}}}{P_t} r_1^\alpha \right) f_{R_1}(r_1) dr_1 \right) \times \\ &\quad \left( \int_0^\infty \int_0^\infty \mathcal{L}_{j\text{-inter}}^{\text{chain}} \left( \frac{\delta_{\text{th}}}{P_t} r_2^\alpha \right) \mathcal{L}_{j\text{-intra}}^{\text{chain}} \left( \frac{\delta_{\text{th}}}{P_t} r_2^\alpha | s_r \right) f_{R_2}(r_2 | s_r) f_{S_r}(s_r) dr_2 ds_r \right), \end{aligned} \quad (28)$$

where  $f_{R_2}(r_2 | s_r) = f_D(r_2, s_r; \sigma^2)$ ,  $r_2 \geq 0$ , and  $f_{S_r}(s_r) = f_S(s_r; \sigma^2)$ ,  $s_r \geq 0$ .

*Proof:* For the D2D link from device  $i$  to  $j$ , the probability of the D2D link from device  $i$  to  $j$  meeting the minimum SINR threshold is

$$\begin{aligned} \mathbb{P}_j^{\text{chain}}(\delta_{\text{th}}) &= \mathbb{E}(\mathbb{P}\{\delta_j > \delta_{\text{th}}\}) \\ &= \mathbb{E}_R \left[ \mathbb{P} \left( h_{ij} > \frac{\delta_{\text{th}}}{P_t} (I_{j\text{-intra}}^{x_r} + I_{j\text{-inter}}^{x_r}) ||x_r + y_j||^\alpha \right) \right] \end{aligned}$$

$$\begin{aligned}
&= \mathbb{E}_R \left[ \mathbb{E} \left[ \exp \left( \frac{\delta_{\text{th}}}{P_t} (I_{j-\text{intra}}^{x_r} + I_{j-\text{inter}}^{x_r}) ||x_r + y_j||^\alpha \right) \right] \right] \\
&\stackrel{(a)}{=} \int_0^\infty \int_0^\infty \mathcal{L}_{j-\text{inter}}^{\text{chain}} \left( \frac{\delta_{\text{th}}}{P_t} r_2^\alpha \right) \mathcal{L}_{j-\text{intra}}^{\text{chain}} \left( \frac{\delta_{\text{th}}}{P_t} r_2^\alpha | s_r \right) f_{R_2}(r_2 | s_r) f_{S_r}(s_r) dr_2 ds_r. \quad (29)
\end{aligned}$$

In (a), we first make a change of variables by setting  $r_2 = ||x_r + y_j||$ , and, then, we perform one de-conditioning in terms of  $r_2$  and another de-conditioning for  $s_r$ , and finally convert the coordinates from Cartesian to polar. Based on the distance distribution, we have  $f_{R_2}(r_2 | s_r) = f_D(r_2, s_r; \sigma^2)$  and  $f_{S_r}(s_r) = f_S(s_r; \sigma^2)$ . Then, since the outage will not occur if and only if the SINR of both links exceed the threshold level, we can obtain (28).  $\blacksquare$

Similar to Corollary 3, we can replace  $\delta_{\text{th}}$  with  $2^{\frac{R}{w_1}} - 1$  in (21) and (29) to obtain the throughput CDF for the two D2D links in the chain motif. To calculate the throughput, we can observe that the chain motif is equivalent to a two-hop network. According to the work in [30], if a non-seeding node is connected to the seeding node through a multi-hop link with length  $l$ , the achievable throughput of the non-seeding device is limited by  $1/l$  times the minimum of all D2D link rates over the multi-hop communication network. Therefore, we can derive the expected throughput of non-seeding devices  $j$  and  $k$  in the following corollaries.

**Corollary 7.** *Since device  $j$  is directly connected to seeding node  $i$ , the expected throughput is*

$$\begin{aligned}
E_{\text{chain}} &= \frac{1}{1} \min \left( \int_0^\infty (1 - (1 - \mathbb{P}_j^{\text{chain}}(2^{\frac{R}{w_1}} - 1))) dR \right) \\
&= \int_0^\infty \int_0^\infty \int_0^\infty \mathcal{L}_{j-\text{inter}}^{\text{chain}} \left( \frac{2^{\frac{R}{w_1}} - 1}{P_t} r_2^\alpha \right) \mathcal{L}_{j-\text{intra}}^{\text{chain}} \left( \frac{2^{\frac{R}{w_1}} - 1}{P_t} r_2^\alpha | s_r \right) f_{R_2}(r_2 | s_r) f_{S_r}(s_r) dr_2 ds_r dR. \quad (30)
\end{aligned}$$

**Corollary 8.** *Since device  $k$  connects to the seeding device  $i$  via a two-hop link, the expected throughput is given by*

$$\begin{aligned}
E'_{\text{chain}} &= \frac{1}{2} \min \left( \int_0^\infty \int_0^\infty \mathcal{L}_{j-\text{inter}}^{\text{star}} \left( \frac{2^{\frac{R}{w_1}} - 1}{P_t} r_1^\alpha \right) \mathcal{L}_{j-\text{intra}}^{\text{star}} \left( \frac{2^{\frac{R}{w_1}} - 1}{P_t} r_1^\alpha | s_r \right) f_{R_1}(r_1) dr_1 dR, \right. \\
&\quad \left. \int_0^\infty \int_0^\infty \int_0^\infty \mathcal{L}_{j-\text{inter}}^{\text{chain}} \left( \frac{2^{\frac{R}{w_1}} - 1}{P_t} r_2^\alpha \right) \mathcal{L}_{j-\text{intra}}^{\text{chain}} \left( \frac{2^{\frac{R}{w_1}} - 1}{P_t} r_2^\alpha | s_r \right) f_{R_2}(r_2 | s_r) f_{S_r}(s_r) dr_2 ds_r dR \right). \quad (31)
\end{aligned}$$

### C. Expected Throughput for Seeding Devices

From the work in [27], conditioned on the distance between the parent point  $x_r \in \Phi_p$  and a typical device at the origin, the distance between the device in cluster  $C_r$  and the typical device

follows a Rician distribution. Equivalently, if we set the condition as the distance  $z = ||x_r - b||$  between the parent point  $x_r$  and the BS  $b$ , the distance  $r_3$  between the devices in the cluster and the BS will also follow a Rician distribution  $f_{R_3}(r_3|z) = f_D(r_3, z; \sigma^2)$ ,  $z, r_3 > 0$ . Similar to (22), we change the coordinates and replace the variables, and, then, the CDF of throughput will be:

$$\begin{aligned} P(R_k < R) &= 1 - \int_{\mathbb{R}^2} \int_{\mathbb{R}^2} \frac{2^{\frac{R}{w_2}} - 1}{P_b} P_n ||x_r + y - b||^\alpha f_Y(y) f_X(x_r) dx_r dy \\ &= 1 - \int_0^\infty \int_0^\infty \frac{2^{\frac{R}{w_2}} - 1}{P_b} P_n r_3^\alpha f_{R_3}(r_3|z) f_Z(z) dr_3 dz, \end{aligned} \quad (32)$$

where  $r_3 = x_r + y - b$ .

According to the distribution of parent points,  $z$  can be interpreted as the distance between the BS and a point which is uniformly distributed in the area. Without loss of generality, we assume that the BS is at the center of a square area of side  $2L$  that contains all devices. Hence, the CDF expression for the distance  $z$  will be:

$$F_Z(z) = \frac{1}{4L^2} \begin{cases} \pi z^2, & 0 \leq z \leq L, \\ \pi z^2 - 4 \left( z^2 \arccos\left(\frac{L}{z}\right) - L\sqrt{z^2 - L^2} \right), & L \leq z \leq \sqrt{2}L, \\ 1, & \sqrt{2}L \leq z. \end{cases} \quad (33)$$

We can then find the corresponding PDF as

$$f_Z(z) = \frac{1}{2L^2} \begin{cases} \pi z, & 0 \leq z \leq L, \\ \pi z - 4z \arccos\left(\frac{L}{z}\right), & L \leq z \leq \sqrt{2}L, \\ 0, & \text{otherwise.} \end{cases} \quad (34)$$

Based on the relationship between the SINR and the expected throughput, we can obtain the expression of the throughput in the next Lemma.

**Lemma 5.** *For seeding devices within the D2D network, the expected throughput is given by*

$$E_{\text{seeding}} = \int_0^\infty \int_0^\infty \int_0^\infty \frac{2^{\frac{R}{w_2}} - 1}{P_b} P_n r_3^\alpha f_{R_3}(r_3|z) f_Z(z) dr_3 dz dR. \quad (35)$$

#### D. Average Throughput per Device in the D2D Network

After obtaining the throughput for each device and the possibility of a three-node motif being either a star or a chain motif, the expected average throughput per device in the D2D network can be derived next.

Table. I. Simulation parameters.

Parameter	Definition	Value
$P_b$	Transmission power of BS	46 dBm
$P_t$	Transmission power of devices	23 dBm
$N$	Number of devices in each cluster	25, 50, 100
$\sigma^2$	Distribution variance	50, 100, 150
$\lambda_p$	Cluster density	5, 10, 20 clusters/km <sup>2</sup>
$w$	Total system bandwidth	20 MHz
$\beta$	Bandwidth parameter	0.6
$\alpha$	Path loss exponent	4
$\delta_{th}$	Minimum SINR requirement	0 dB
$\theta$	Probability of being a star motif	1/3
$I$	Noise spectral density	-174 dBm/Hz
$I$	Simulation area	1 km $\times$ 1 km

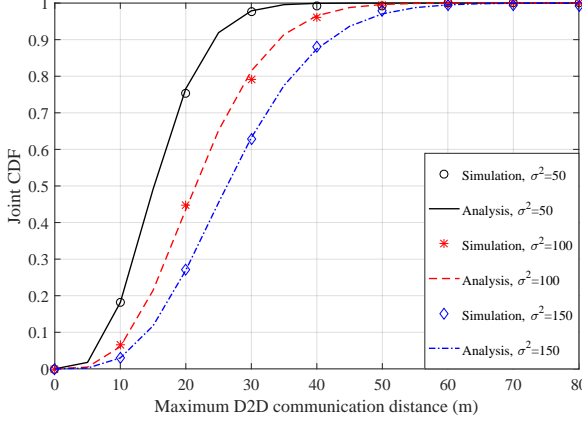
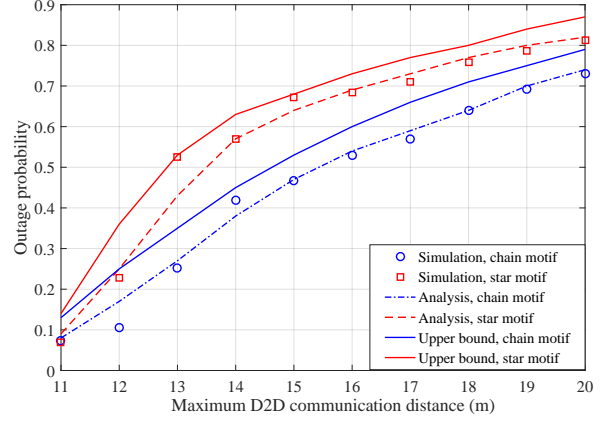
**Corollary 9.** *Based on (23), (30), (31), as well as (35), and the possibilities of a three-node motif being either a star or a chain motif, the average throughput per device will be:*

$$\begin{aligned}
 E_R &= \frac{2c_o^{\text{star}} E_{\text{star}} + c_o^{\text{star}} E_{\text{seeding}} + c_o^{\text{chain}} E_{\text{chain}} + c_o^{\text{chain}} E'_{\text{chain}} + c_o^{\text{chain}} E_{\text{seeding}} + E_{\text{seeding}}}{N} \\
 &= \frac{2c_o^{\text{star}} E_{\text{star}} + c_o^{\text{chain}} E_{\text{chain}} + c_o^{\text{chain}} E'_{\text{chain}} + (c_o + 1) E_{\text{seeding}}}{N}.
 \end{aligned} \tag{36}$$

We can observe that the average throughput per device in the content dissemination network is dependent on the same factors on which the  $Z$ -scores of both the star and chain motifs depend, namely, the distribution variance, the number of devices, and the maximum allowable distance. Thus, both the system throughput and  $Z$ -score for motifs are functions of the same network parameters and, hence, the BS can collect data on  $Z$ -scores of chain and star motifs and the system throughput corresponding to the same settings. This data can help understand how the dissemination performance changes as the occurrence of different motifs varies and further identify  $Z$ -score regions, which map to the optimal content dissemination performance, for both chain and star motifs, as will also be evident from the subsequent simulation results.

## V. SIMULATION RESULTS

Next, we present rigorous simulation results to validate the analytical derivations and show the relationship between the occurrence of motifs and the content dissemination performance in D2D-enabled cellular networks. In particular, we consider that wireless devices are distributed within a square area of 1 km  $\times$  1 km. Also, for each D2D link, the transmitter is chosen

Fig. 4. Joint CDF versus distance threshold  $s_{th}$ .Fig. 5. Outage probability versus distance threshold  $s_{th}$ .

randomly. To observe the impacts of different network topology parameters on the occurrence of motifs and the system throughput, we change the distribution variance and the cluster density. Simulation parameters are summarized in Table I.

Fig. 4 shows the joint CDF  $\mathbb{P}_{S,S}$  of a group of three devices being a three-node motif versus the communication distance  $s_{th}$  for systems with  $\lambda_p = 20$  cluster/km<sup>2</sup> and  $\sigma^2 = 50, 100, 150$ . As shown in Fig. 4, we can observe that the simulation results corroborate the analytical results in Theorem 1. Moreover, as  $s_{th}$  increases,  $\mathbb{P}_{S,S}$  increases. But, the increase varies differently for different D2D systems. In particular, to achieve  $\mathbb{P}_{S,S} = 1$ , the  $s_{th}$  for the D2D system with  $\sigma^2 = 50$  should be around 40 m, while the ones of systems with  $\sigma^2 = 100, 150$  are, respectively, close to 50 m and 60 m. This is due to the fact that, in the system with a smaller distribution variance, devices are more likely to form three-node motifs. Furthermore, for a fixed distance threshold  $s_{th}$ , we can observe that the system with a lower variance will lead to a higher probability  $\mathbb{P}_{S,S}$ . For example, when  $s_{th} = 20$  m, the values of  $\mathbb{P}_{S,S}$  are approximately 0.75, 0.45, and 0.28 for the systems with  $\sigma^2 = 50, 100, 150$ .

Fig. 5 shows the outage probability, for chain and star motifs, versus the D2D communication distance  $s_{th}$  with  $\delta_{th} = 0$  dB,  $\sigma^2 = 100$ , and  $N = 25$  in each cluster. As illustrated in Fig. 5, the simulation results validate the analytical results in Theorems 2 and 3. Moreover, the lower bounds for the intra- and inter-cluster interference in Corollaries 1, 2, 5 and 6 can lead to upper bounds of outage probabilities for both motifs. Moreover, we can observe that, as  $s_{th}$  increases, the outage probabilities for both motifs will increase. This is due to the fact that as the maximum distance increases, the D2D system is more likely to have more motifs, leading to more interference and thereby a lower SINR.

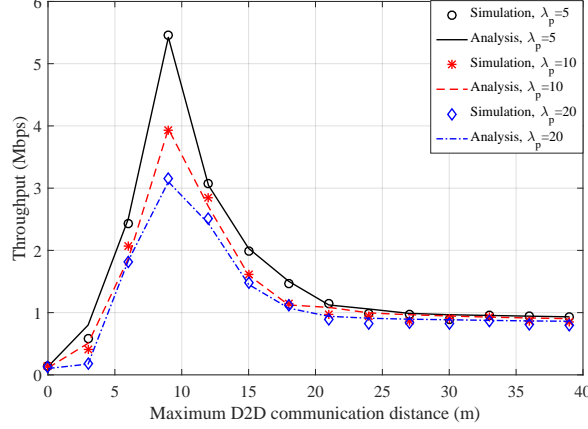


Fig. 6. Average data per device versus the distance threshold  $s_{th}$ .

Fig. 6 shows the average throughput per device when  $\sigma^2 = 100$ ,  $\lambda_p = 5, 10, 20$ , and  $N = 50$ . In Fig. 6, we can observe that the simulation results of average throughput corroborate the analytical derivations in Corollary 9. Moreover, Fig. 6 shows that the cluster density  $\lambda_p$  plays an important role in determining the content dissemination performance. In particular, when  $s_{th}$  is small, the system with a smaller cluster density  $\lambda_p$  will have a higher throughput. However, when  $s_{th}$  is above 30 m, the throughput of D2D systems with lower cluster densities is slightly better than the counterpart for systems with higher cluster densities. In fact, when  $s_{th}$  is very small, both motifs barely exist in the networks and, thus, D2D links will experience less intra-cluster interference. In this case, the system performance mainly depends on the inter-cluster interference. Therefore, a system with a lower cluster density tends to have a better performance than the one with a higher density. However, when  $s_{th}$  is larger, more and more three-node motifs will appear in the network, increasing both inter- and intra-cluster interference. From the analytical results in Section IV, we can observe that when the  $s_{th}$ ,  $N$ , and  $\sigma^2$  are fixed, intra-cluster interference will be the same for systems with different  $\lambda_p$ . But, due to the different cluster densities, the inter-cluster interference will be different. We can observe that, when  $s_{th}$  increases to 25 m, the average throughput is equal for all  $\lambda_p$ . This is due to the fact that, in such a case, the intra-cluster interference has a dominant effect on the system performance.

Fig. 7 presents the  $Z$ -scores for the chain and star motifs versus the distribution variance  $\sigma^2$ . We can observe that, as the distribution variance  $\sigma^2$  increases, the  $Z$ -scores for both chain and star motifs will decrease. The reason is that, for a fixed  $s_{th}$ , as the variance  $\sigma^2$  increases, both motifs are less likely to occur in the network. Moreover, we can observe that  $Z$ -scores of chain motifs are higher than the counterparts for star motifs, indicating that chain motifs

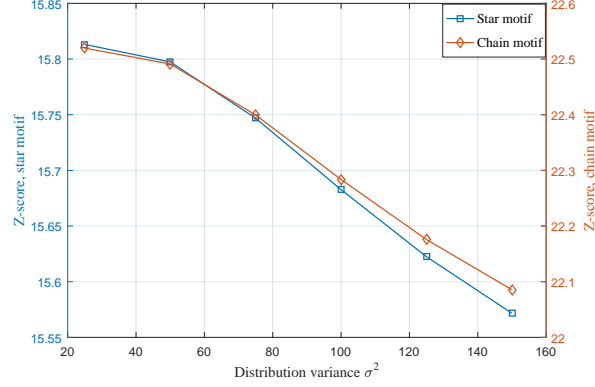


Fig. 7. Z-scores for the chain and star motifs versus the distribution variance  $\sigma^2$ .

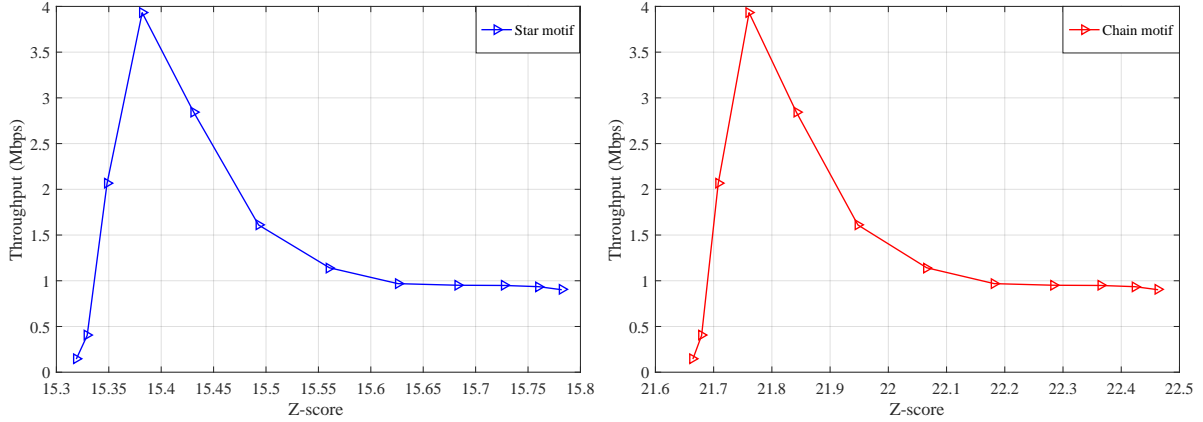


Fig. 8. Average throughput per device versus Z-score for the star and chain motifs.

are more likely to occur in network. It can be explained that star motifs need more restrictive requirements, i.e., two different D2D links sharing the same seeding device. By combining the results of Fig. 6 and Fig. 7 with the analytical derivations in Section III and Section IV, we can see that both the average throughput per device and the Z-scores for the motifs are dependent on the same factors, i.e.,  $\sigma^2$  and  $s_{th}$ .

Fig. 8 shows the average throughput per device versus the Z-scores for the chain and star motifs. Here, we consider a network with  $\lambda_p = 10$  clusters/km<sup>2</sup>,  $\sigma^2 = 100$  and  $N = 50$ . Moreover, we change the value of  $s_{th}$  so that we can change the Z-scores for both motifs as well as the system throughput. From Fig. 8, we can see that, for both motifs, the average throughput is a concave function with respect to the Z-scores for both motifs. Moreover, there exists Z-score regions for both chain and star motifs that lead to a higher throughput than points in other Z-score regions. This stems from the tradeoff between received signal power over the D2D communication links and the interference introduced from the increased number of D2D links. In addition, the optimal Z-score regions will be different for star and chain motifs. For

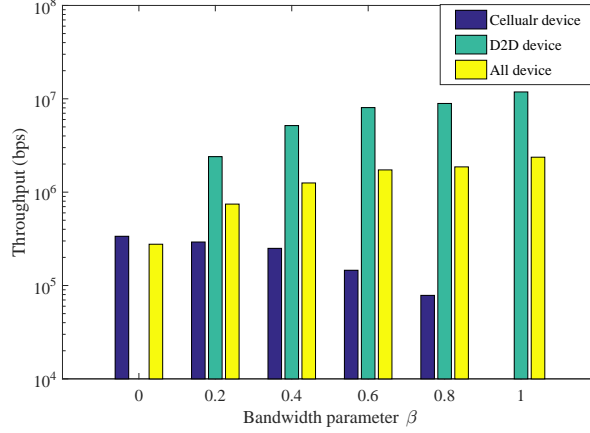


Fig. 9. Average throughput of D2D, cellular, and all devices versus bandwidth parameter  $\beta$ .

example, for chain motifs, the  $Z$ -score region where the network can achieve at least 2 Mbps throughput is from 21.71 to 21.92, and the counterpart for the star motif is from 15.35 to 15.47.

Fig. 9 shows the average throughput for D2D and cellular devices under different bandwidth parameter  $\beta$ , when  $\sigma^2 = 100$ ,  $s_{th} = 15$  m, and  $\lambda_p = 10$  clusters/km<sup>2</sup>. We can observe that as the bandwidth parameter increases, the average average D2D throughput will increase while the throughput for cellular devices decreases. We can conclude that the system performance is mainly determined by the average throughput of D2D devices. Therefore, when designing a D2D system, the bandwidth parameter  $\beta$  should be properly chosen so that the D2D-enabled cellular system can achieve the target performance.

From the simulation results shown in Figs. 6-9, we can observe that, as long as the operator knows the  $Z$ -scores of the chain and star motifs appearing in the D2D communication networks, the achievable content dissemination performance, captured by the average throughput, can be predictable. The predictable throughput can enable the operator to find the optimal  $Z$ -score regions which can achieve a high dissemination performance. Hence, when using D2D communications for content dissemination, the operators can identify the proper clusters to achieve a targeted performance by verifying whether the  $Z$ -score is in the optimal region. Furthermore, because of the relationship between the  $Z$ -score and the expected number of occurrences of chain and star motifs, we can also determine the number of seeding devices in each identified cluster. As such, based on the relationship between motif occurrence and content dissemination performance, the operators can decide on how to identify proper clusters to leverage D2D communications and further determine the number of seeding devices in each identified cluster for the optimal content dissemination policy.

## VI. CONCLUSION

In this paper, we have proposed a novel DNA framework to explore frequent communication patterns across D2D users, known as spatial motifs, to optimize content dissemination in emerging cellular networks. In particular, we have utilized the stochastic geometry to derive the analytical results of the frequency of occurrence for two common types of motifs composed of three devices, and the performance metrics for each motif in the D2D-enabled clustered network. Simulation results have corroborated the analytical derivations and shown the impact of system topologies on the occurrence of motif and the average throughput. More importantly, the simulation results have shed light on the relationship between the average throughput and the motifs appearing in the D2D network. The derived relationship can be used by network operators to obtain the statistical significance regions for different motifs observed in the network, and to determine the content dissemination strategy – e.g., allocating bandwidth to D2D links, determining number of seeding nodes, etc – in future cellular networks. Therefore, by implementing the proposed framework, the operator can obtain guidelines for designing effective content dissemination strategies in D2D-enabled cellular networks.

## APPENDIX

### A. Proof of Lemma 1

We conduct the Laplace transform of the intra-cluster interference of device  $j$  as

$$\begin{aligned}
\mathcal{L}_{j\text{-intra}}^{\text{star}}(s) &\stackrel{(a)}{=} \mathbb{E} \left[ \exp \left( -s \sum_{y \in \mathcal{T}_{x_r} \setminus y_i} P_t h_{yj} \|y_j - y\|^{-\alpha} \right) \right] \\
&= \mathbb{E}_{\mathcal{T}_{x_r}} \left[ \prod_{y \in \mathcal{T}_{x_r} \setminus y_i} \mathbb{E}_{h_{yj}} [\exp(-s P_t h_{yj} \|y - y_j\|^{-\alpha})] \right] \\
&\stackrel{(b)}{=} \mathbb{E}_{\mathcal{T}_{x_r}} \left[ \prod_{y \in \mathcal{T}_{x_r} \setminus y_i} \frac{1}{1 + s P_t \|y - y_j\|^{-\alpha}} \right] \\
&\stackrel{(c)}{=} \sum_{k=0}^{N_m-1} \left( \mathbb{E} \left[ \frac{1}{1 + s P_t \|y - y_j\|^{-\alpha}} \right] \right)^k \times \underbrace{\binom{N_m-1}{k} (\mathbb{P}_{S,S})^k (1 - \mathbb{P}_{S,S})^{N_m-1-k}}_{\mathbb{P}(n=k)} \\
&\stackrel{(d)}{=} \sum_{k=0}^{N_m-1} \left( \int_0^\infty \frac{1}{1 + s P_t v_1^{-\alpha}} f_{V_1}(v_1) dv_1 \right)^k \times \binom{N_m-1}{k} (\mathbb{P}_{S,S})^k (1 - \mathbb{P}_{S,S})^{N_m-1-k}
\end{aligned}$$

$$\begin{aligned}
&= \sum_{k=0}^{N_m-1} \binom{N_m-1}{k} \left( \int_0^\infty \frac{1}{1+sP_t z_1^{-\alpha}} f_{V_1}(v_1) dv_1 \mathbb{P}_{S,S} \right)^k \times (1 - \mathbb{P}_{S,S})^{N_m-1-k} \\
&\stackrel{(e)}{=} \left( \int_0^\infty \frac{1}{1+sP_t v_1^{-\alpha}} f_{V_1}(v_1) dv_1 \mathbb{P}_{S,S} + 1 - \mathbb{P}_{S,S} \right)^{N_m-1}, \tag{37}
\end{aligned}$$

where (a) is the definition of Laplace transformation, (b) follows from assumption of Rayleigh fading channel and the channel gain  $h_{yj} \sim \exp(1)$ , and the transformation in (c) is due to the fact the locations of devices within the cluster are i.i.d. variables. We substitute  $v_1$  with  $\|y - y_1\|$  and change the Cartesian to the polar coordinates in (d). Since both  $y$  and  $y_1$  are i.i.d., and follow zero mean complex Gaussian distribution with variance  $\sigma^2$ , we have the PDF of  $v_1$ :  $f_{V_1}(v_1) = f_S(v_1; 2\sigma^2)$ ,  $v_1 \geq 0$ . The change in (e) is based upon the binomial expansion of a power of a sum [31].

### B. Proof of Corollary 1

The lower bound could be given by:

$$\begin{aligned}
\mathcal{L}_{j\text{-intra}}^{\text{star}}(s) &= \left( \int_0^\infty \frac{1}{1+sP_t v_1^{-\alpha}} f_S(v_1; 2\sigma^2) dv_1 \mathbb{P}_{S,S} + 1 - \mathbb{P}_{S,S} \right)^{N_m-1} \\
&= \left( 1 - \left( 1 - \int_0^\infty \frac{1}{1+sP_t v_1^{-\alpha}} f_S(v_1; 2\sigma^2) dv_1 \right) \mathbb{P}_{S,S} \right)^{N_m-1} \\
&\stackrel{(a)}{=} \left( 1 - \left( \int_0^\infty \frac{sP_t}{v_1^\alpha + sP_t} f_S(v_1; 2\sigma^2) dv_1 \right) \mathbb{P}_{S,S} \right)^{N_m-1} \\
&\stackrel{(b)}{\geq} 1 - (N_m - 1) \int_0^\infty \frac{sP_t}{v_1^\alpha + sP_t} f_S(v_1; 2\sigma^2) dv_1 \mathbb{P}_{S,S}, \tag{38}
\end{aligned}$$

where the changes in (a) is replacing 1 with  $\int_0^\infty f_S(v_1; 2\sigma^2) dv_1$ . In (a), due to the fact  $0 \leq \frac{sP_t}{v_1^\alpha + sP_t} \leq 1$  and the monotony of integral, we can have  $0 \leq \int_0^\infty \frac{sP_t}{v_1^\alpha + sP_t} f_S(z_1; 2\sigma^2) dz_1 \leq \int_0^\infty f_S(v_1; 2\sigma^2) dv_1 = 1$ . Also, since  $\mathbb{P}_{S,S} \in (0, 1)$ , the product of  $\mathbb{P}_{S,S}$  and  $\int_0^\infty \frac{sP_t}{v_1^\alpha + sP_t} f_S(z_1; 2\sigma^2) dz_1$  is in  $(0, 1)$ . In (b), based on the Bernoulli inequality [29], we are able to derive the lower bound for the intra-cluster interference as (38).

### C. Proof of Lemma 2

We can conduct Laplace transform for the inter-cluster interference as

$$\mathcal{L}_{j\text{-inter}}^{\text{star}}(s) \stackrel{(a)}{=} \mathbb{E} \left[ \exp \left( -s \sum_{x \in \Phi_p \setminus x_r} \sum_{y' \in \mathcal{T}_x} P_t h_{yj} \|x + y' - x_r - y_j\|^{-\alpha} \right) \right]$$

$$\begin{aligned}
&= \mathbb{E}_{\Phi_p} \left[ \prod_{x \in \Phi_p \setminus x_r} \mathbb{E}_{\mathcal{T}_x} \left[ \prod_{y' \in \mathcal{T}_x} \mathbb{E}_{h_{yj}} [\exp(-sP_t h_{yj} \|x + y' - x_r - y_j\|^{-\alpha})] \right] \right] \\
&\stackrel{(b)}{=} \mathbb{E}_{\Phi_p} \left[ \prod_{x \in \Phi_p \setminus x_r} \mathbb{E}_{\mathcal{T}_x} \left[ \prod_{y' \in \mathcal{T}_x} \frac{1}{1 + sP_t \|x + y' - x_r - y_j\|^{-\alpha}} \right] \right] \\
&\stackrel{(c)}{=} \mathbb{E}_{\Phi_p} \left[ \prod_{x \in \Phi_p \setminus x_r} \sum_{k=0}^{N_m} \left( \mathbb{E}_{\mathcal{T}_x} \left[ \frac{1}{1 + sP_t \|x + y' - x_r - y_j\|^{-\alpha}} \right] \right)^k \times \right. \\
&\quad \left. \underbrace{\binom{N_m}{k} (\mathbb{P}_{S,S})^k (1 - \mathbb{P}_{S,S})^{N_m-k}}_{\mathbb{P}(n=k)} \right] \\
&\stackrel{(d)}{=} \mathbb{E}_{\Phi_p} \left[ \prod_{x \in \Phi_p \setminus x_r} \sum_{k=0}^{N_m} \left( \int_{\mathbb{R}^2} \frac{1}{1 + sP_t \|x + z_2\|^{-\alpha}} f_{Z_2}(z_2) dz_2 \right)^k \times \binom{N_m}{k} (\mathbb{P}_{S,S})^k (1 - \mathbb{P}_{S,S})^{N_m-k} \right] \\
&\stackrel{(e)}{=} \exp \left( -\lambda_p \int_{\mathbb{R}^2} \left( 1 - \sum_{k=0}^{N_m} \left( \int_{\mathbb{R}^2} \frac{1}{1 + sP_t \|x + z_2\|^{-\alpha}} f_{Z_2}(z_2) dz_2 \right)^k \times \binom{N_m}{k} (\mathbb{P}_{S,S})^k (1 - \mathbb{P}_{S,S})^{N_m-k} \right) dx \right) \\
&\stackrel{(f)}{=} \exp \left( -\lambda_p \int_{\mathbb{R}^2} \left( 1 - \left( \int_{\mathbb{R}^2} \frac{1}{1 + sP_t \|x + z_2\|^{-\alpha}} f_{Z_2}(z_2) dz_2 \mathbb{P}_{S,S} + 1 - \mathbb{P}_{S,S} \right)^{N_m} \right) dx \right) \\
&\stackrel{(g)}{=} \exp \left( -\lambda_p 2\pi \int_0^\infty \left( 1 - \left( \int_0^\infty \frac{1}{1 + sP_t v_2^{-\alpha}} f_{V_2}(v_2|t) dv_2 \mathbb{P}_{S,S} + 1 - \mathbb{P}_{S,S} \right)^{N_m} \right) t dt \right), \tag{39}
\end{aligned}$$

where  $f_{V_2}(v_2|t) = f_D(v_2, t; 3\sigma^2)$ ,  $v_2 \geq 0$ . The changes in (a), (b), (c), and (f) follow the same reasons with (a), (b), (c) and (e) in (37). In (d), we assume  $z_2 = y' - x_r - y_i$ , where  $y'$ ,  $x_r$ , and  $y_1$  are i.i.d. and follow zero mean complex Gaussian distribution with variance  $\sigma^2$ . Hence,  $z_2$  follows zero mean complex Gaussian distribution with variance  $3\sigma^2$ . (e) can be explained by the probability generation function (PGFL) of PPP [32]. In (g), we substitute the variable  $v_2$  with  $\|x + z_2\|$  and convert the coordinates from Cartesian to polar.

#### D. Proof of Corollary 2

We first analyse one part of the equation in (39), and then obtain the final inequation. Similar to Appendix B, we can have

$$\left( \int_0^\infty \frac{1}{1 + sP_t v_2^{-\alpha}} f_R(v_2|t) dv_2 \mathbb{P}_{S,S} + 1 - \mathbb{P}_{S,S} \right)^{N_m} \geq 1 - N_m \int_0^\infty \frac{sP_t}{v_2^\alpha + sP_t} f_R(v_2|t) dv_2 \mathbb{P}_{S,S}. \tag{40}$$

Based on that, we can derive

$$\begin{aligned}
\mathcal{L}_{j\text{-inter}}^{\text{star}}(s) &= \exp \left( -\lambda_p 2\pi \int_0^\infty \left( 1 - \left( \int_0^\infty \frac{1}{1 + sP_t v_2^{-\alpha}} f_R(v_2|t) dv_2 \mathbb{P}_{S,S} + 1 - \mathbb{P}_{S,S} \right)^{N_m} \right) t dt \right) \\
&\geq \exp \left( -\lambda_p 2\pi N_m \int_0^\infty \left( \int_0^\infty \frac{sP_t}{v_2^\alpha + sP_t} f_R(v_2|t) dv_2 \mathbb{P}_{S,S} \right) t dt \right) \\
&\stackrel{(a)}{=} \exp \left( -\lambda_p 2\pi N_m \int_0^\infty \frac{sP_t}{v_2^\alpha + sP_t} v_2 dv_2 \mathbb{P}_{S,S} \right) \\
&\stackrel{(b)}{=} \exp \left( -\lambda_p 2\pi N_m \frac{(sP_t)^{\frac{2}{\alpha}} \pi \csc(\frac{2\pi}{\alpha})}{\alpha} \mathbb{P}_{S,S} \right), \tag{41}
\end{aligned}$$

where the change in (a) depends on the fact of Rice distribution where  $\int_0^\infty f_R(v_2|t) t dt = v_2$ .

The changes in (b) are with the aid of Mathematica.

### E. Proof of Lemma 3

We conduct the Laplace transform of the intra-cluster interference as

$$\begin{aligned}
\mathcal{L}_{j\text{-inter}}^{\text{chain}}(s|s_r) &\stackrel{(a)}{=} \mathbb{E} \left[ \exp \left( -s \sum_{y \in \mathcal{T}_x \setminus y_i} P_t h_{yj} ||x_r + y||^{-\alpha} \right) \right] \\
&= \mathbb{E}_{\mathcal{T}_x} \left[ \prod_{y \in \mathcal{T}_x \setminus y_i} \mathbb{E}_{h_{yj}} [\exp(-s P_t h_{yj} ||x_r + y||^{-\alpha})] \right] \\
&\stackrel{(b)}{=} \mathbb{E}_{\mathcal{T}_x} \left[ \prod_{y \in \mathcal{T}_x \setminus y_j} \mathbb{E}_{h_{yj}} \left[ \frac{1}{1 + sP_t ||x_r + y||^{-\alpha}} \right] \right] \\
&\stackrel{(c)}{=} \sum_{k=0}^{N_m-1} \left( \int_{\mathbb{R}^2} \frac{1}{1 + sP_t ||x_r + y||^{-\alpha}} f_Y(y) dy \right)^k \times \underbrace{\binom{N_m-1}{k} (\mathbb{P}_{S,S})^k (1 - \mathbb{P}_{S,S})^{N_m-1-k}}_{\mathbb{P}(n=k)} \\
&= \sum_{k=0}^{N_m-1} \binom{N_m-1}{k} \left( \int_{\mathbb{R}^2} \frac{1}{1 + sP_t ||x_r + y||^{-\alpha}} f_Y(y) dy \mathbb{P}_{S,S} \right)^k \times (1 - \mathbb{P}_{S,S})^{N_m-1-k} \\
&\stackrel{(d)}{=} \left( \int_{\mathbb{R}^2} \frac{1}{1 + sP_t ||x_r + y||^{-\alpha}} f_Y(y) dy \mathbb{P}_{S,S} + 1 - \mathbb{P}_{S,S} \right)^{N_m-1} \\
&\stackrel{(e)}{=} \left( \int_0^\infty \frac{1}{1 + sP_t v_3^{-\alpha}} f_{V_3}(v_3|s_r) dv_3 \mathbb{P}_{S,S} + 1 - \mathbb{P}_{S,S} \right)^{N_m-1}, \tag{42}
\end{aligned}$$

where  $f_R(v_3|s_r) = f_D(v_3, s_r; \sigma^2)$ . The changes in (a), (b), (c), and (d) follow the same reasons with (a), (b), (c) and (e) in (37). In (e), we change the variables by using  $v_3 = ||x_r + y||$  and convert from Cartesian to polar coordinates.

### F. Proof of Lemma 4

We conduct Laplace transform for the inter-cluster interference as

$$\begin{aligned}
\mathcal{L}_{j\text{-inter}}^{\text{chain}}(s) &\stackrel{(a)}{=} \mathbb{E} \left[ \exp \left( -s \sum_{x \in \Phi_p \setminus x_r} \sum_{y' \in \mathcal{T}_x} P_t h_{yj} \|x + y'\|^{-\alpha} \right) \right] \\
&= \mathbb{E}_{\Phi_p} \left[ \prod_{x \in \Phi_p \setminus x_r} \mathbb{E}_{\mathcal{T}_x} \left[ \prod_{y' \in \mathcal{N}_x} \mathbb{E}_{h_{yj}} [\exp(-s P_t h_{yi} \|x + y'\|^{-\alpha})] \right] \right] \\
&\stackrel{(b)}{=} \mathbb{E}_{\Phi_p} \left[ \prod_{x \in \Phi_p \setminus x_r} \mathbb{E}_{\mathcal{T}_x} \left[ \prod_{y' \in \mathcal{N}_x} \frac{1}{1 + s P_t \|x + y'\|^{-\alpha}} \right] \right] \\
&\stackrel{(c)}{=} \mathbb{E}_{\Phi_p} \left[ \prod_{x \in \Phi_p \setminus x_r} \sum_{k=0}^{N_m} \left( \int_{\mathbb{R}^2} \frac{1}{1 + s P_t \|x + y'\|^{-\alpha}} f_Y(y') dy' \right)^k \times \underbrace{\binom{N_m}{k} (\mathbb{P}_{S,S})^k (1 - \mathbb{P}_{S,S})^{N_m-k}}_{\mathbb{P}(n=k)} \right] \\
&\stackrel{(d)}{=} \exp \left( -\lambda_p \int_{\mathbb{R}^2} \left( 1 - \sum_{k=0}^{N_m} \left( \int_{\mathbb{R}^2} \frac{1}{1 + s P_t \|x + y'\|^{-\alpha}} f_Y(y') dy' \right)^k \right. \right. \\
&\quad \left. \left. \times \binom{N_m}{k} (\mathbb{P}_{S,S})^k (1 - \mathbb{P}_{S,S})^{N_m-k} \right) dx \right) \\
&\stackrel{(e)}{=} \exp \left( -\lambda_p \int_{\mathbb{R}^2} \left( 1 - \left( \int_{\mathbb{R}^2} \frac{1}{1 + s P_t \|x + y'\|^{-\alpha}} f_Y(y') dy' \mathbb{P}_{S,S} + 1 - \mathbb{P}_{S,S} \right)^{N_m} \right) dx \right) \\
&\stackrel{(f)}{=} \exp \left( -\lambda_p 2\pi \int_0^\infty \left( 1 - \left( \int_0^\infty \frac{1}{1 + s P_t v_4^{-\alpha}} f_{V_4}(v_4|t) dv_4 \mathbb{P}_{S,S} + 1 - \mathbb{P}_{S,S} \right)^{N_m} \right) t dt \right), \tag{43}
\end{aligned}$$

where  $f_{V_4}(v_4|t) = f_D(v_4, t; \sigma^2)$ . The changes in (a), (b), (c) (d), and (e) follow the same reasons with (a), (b), (c), (d), and (e) in (39). In (f), we change the variables by using  $v_4 = \|x + y'\|$  and convert from Cartesian to polar coordinates.

### REFERENCES

- [1] T. Zeng, O. Semiari, and W. Saad, "Exploring spatial motifs for device-to-device network analysis (DNA) in 5G networks," in *Proc. of IEEE Asilomar Conference on Signals, Systems and Computers*, Pacific Grove, CA, Oct. 2017.
- [2] Cisco. Cisco visual networking index: Global mobile data traffic forecast update, 2016 to 2021 white paper, 2017.
- [3] A. Asadi, Q. Wang, and V. Mancuso, "A survey on device-to-device communication in cellular networks," *IEEE Communications Surveys & Tutorials*, vol. 16, no. 4, pp. 1801–1819, Fourthquarter 2014.
- [4] J. Liu, N. Kato, J. Ma, and N. Kadowaki, "Device-to-device communication in LTE-advanced networks: A survey," *IEEE Communications Surveys & Tutorials*, vol. 17, no. 4, pp. 1923–1940, Fourthquarter 2015.
- [5] M. Mozaffari, W. Saad, M. Bennis, and M. Debbah, "Unmanned aerial vehicle with underlaid device-to-device communications: Performance and tradeoffs," *IEEE Transactions on Wireless Communications*, vol. 15, no. 6, pp. 3949–3963, Jun. 2016.

- [6] B. Bai, L. Wang, Z. Han, W. Chen, and T. Svensson, "Caching based socially-aware D2D communications in wireless content delivery networks: A hypergraph framework," *IEEE Wireless Communications*, vol. 23, no. 4, pp. 74–81, Aug. 2016.
- [7] O. Semiari, W. Saad, S. Valentin, M. Bennis, and H. V. Poor, "Context-aware small cell networks: How social metrics improve wireless resource allocation," *IEEE Transactions on Wireless Communications*, vol. 14, no. 11, pp. 5927–5940, Nov. 2015.
- [8] Y. Zhao, W. Song, and Z. Han, "Social-aware data dissemination via device-to-device communications: Fusing social and mobile networks with incentive constraints," *IEEE Transactions on Services Computing*, accepted and to appear, 2017.
- [9] R. Agarwal, V. Gauthier, M. Becker, T. Toukabrignes, and H. Afifi, "Large scale model for information dissemination with device to device communication using call details records," *Computer Communications*, vol. 59, pp. 1–11, Mar. 2015.
- [10] Z. Wu, L. Wang, G. Araniti, and Z. Han, "Exploiting social-interest interactions on user clustering and content dissemination in device-to-device communications," in *IEEE/CIC International Conference on Communications in China (ICCC)*, Shenzhen, China, Nov. 2015.
- [11] Y. Meng, C. Jiang, H.-H. Chen, and Y. Ren, "Cooperative device-to-device communications: Social networking perspectives," *IEEE Network*, vol. 31, no. 3, May/June 2017.
- [12] X. Lin, J. G. Andrews, and A. Ghosh, "Spectrum sharing for device-to-device communication in cellular networks," *IEEE Transactions on Wireless Communications*, vol. 13, no. 12, pp. 6727–6740, Dec. 2014.
- [13] S. Andreev, O. Galinina, A. Pyattaev, K. Johnsson, and Y. Koucheryavy, "Analyzing assisted offloading of cellular user sessions onto D2D links in unlicensed bands," *IEEE Journal on Selected Areas in Communications*, vol. 33, no. 1, pp. 67–80, Jan. 2015.
- [14] M. Afshang, H. S. Dhillon, and P. H. J. Chong, "Fundamentals of cluster-centric content placement in cache-enabled device-to-device networks," *IEEE Transactions on Communications*, vol. 64, no. 6, pp. 2511–2526, Jun. 2016.
- [15] A. H. Sakr and E. Hossain, "Cognitive and energy harvesting-based d2d communication in cellular networks: Stochastic geometry modeling and analysis," *IEEE Transactions on Communications*, vol. 63, no. 5, pp. 1867–1880, May 2015.
- [16] E. Baştuğ, M. Bennis, M. Kountouris, and M. Debbah, "Cache-enabled small cell networks: Modeling and tradeoffs," *EURASIP Journal on Wireless Communications and Networking*, vol. 2015, no. 1, p. 41, Feb. 2015.
- [17] X. Lin, R. Ratasuk, A. Ghosh, and J. G. Andrews, "Modeling, analysis, and optimization of multicast device-to-device transmissions," *IEEE Transactions on Wireless Communications*, vol. 13, no. 8, pp. 4346–4359, Aug. 2014.
- [18] J. Dai, J. Liu, Y. Shi, S. Zhang, and J. Ma, "Analytical modeling of resource allocation in D2D overlaying multi-hop multi-channel uplink cellular networks," *IEEE Transactions on Vehicular Technology*, vol. 66, no. 8, pp. 6633–6644, Aug. 2017.
- [19] B. Zhou, H. Hu, S.-Q. Huang, and H.-H. Chen, "Intracluster device-to-device relay algorithm with optimal resource utilization," *IEEE Transactions on Vehicular Technology*, vol. 62, no. 5, pp. 2315–2326, Jun. 2013.
- [20] M. Haenggi, *Stochastic geometry for wireless networks*. Cambridge University Press, 2012.
- [21] E. Frlan, "Direct communication wireless radio system," Apr. 4 2000, US Patent 6,047,178.
- [22] H. Ding, S. Ma, and C. Xing, "Feasible D2D communication distance in D2D-enabled cellular networks," in *Proc. of IEEE International Conference on Communication Systems (ICCS)*, Macau, China, Nov. 2014.
- [23] R. Milo, S. Shen-Orr, S. Itzkovitz, N. Kashtan, D. Chklovskii, and U. Alon, "Network motifs: simple building blocks of complex networks," *Science*, vol. 298, no. 5594, pp. 824–827, Oct. 2002.
- [24] U. Alon, "Network motifs: theory and experimental approaches," *Nature Reviews Genetics*, vol. 8, no. 6, pp. 450–461, Jun. 2007.
- [25] E. D. Kolaczyk, *Statistical Analysis of Network Data Methods and Models*. Springer, 2009.
- [26] Q. Zhang, W. Saad, W. Bennis, and M. Debbah, "Network formation game for multi-hop wearable communications over millimeter wave frequencies," in *Proc. of IEEE Global Communications Conference (GLOBECOM)*, Singapore, Dec. 2017.
- [27] M. Afshang, H. S. Dhillon, and P. H. J. Chong, "Modeling and performance analysis of clustered device-to-device networks," *IEEE Transactions on Wireless Communications*, vol. 15, no. 7, pp. 4957–4972, Jul. 2016.
- [28] M. K. Simon, *Probability distributions involving Gaussian random variables: A handbook for engineers and scientists*. Springer Science & Business Media, 2007.
- [29] Y. C. Li and C. C. Yeh, "Some equivalent forms of bernoulli inequality: A survey," *Applied Mathematics*, vol. 4, no. 07, pp. 1070–1093, Jun. 2013.
- [30] M. Sikora, J. N. Laneman, M. Haenggi, D. J. Costello, and T. E. Fuja, "Bandwidth-and power-efficient routing in linear wireless networks," *IEEE Transactions on Information Theory*, vol. 52, no. 6, pp. 2624–2633, Jun. 2006.
- [31] J. Harris and H. Stöcker, *Handbook of mathematics and computational science*. Springer Science & Business Media, 1998.
- [32] S. Chiu, D. Stoyan, W. S. Kendall, and J. Mecke, *Stochastic geometry and its applications*. John Wiley & Sons, 2013.